








RESEARCH ARTICLE

Non-invasive point-of-care optical technique for continuous in vivo assessment of microcirculatory function: Application to a preclinical model of early sepsis

Rasa Eskandari^{1,2}  | Stephanie Milkovich³  | Farah Kamar^{1,2}  |
Daniel Goldman¹  | Donald G. Welsh^{3,4}  | Christopher G. Ellis^{1,3}  |
Mamadou Diop^{1,2} 

¹Department of Medical Biophysics, Western University, London, Ontario, Canada

²Imaging Program, Lawson Health Research Institute, London, Ontario, Canada

³Robarts Research Institute, Western University, London, Ontario, Canada

⁴Department of Physiology and Pharmacology, Western University, London, Ontario, Canada

Correspondence

Rasa Eskandari and Mamadou Diop, Department of Medical Biophysics, Western University, London, ON N6A 3K7, Canada.
Email: reskand2@uwo.ca and mdiop@uwo.ca

Funding information

Canadian Government | Canadian Institutes of Health Research (CIHR), Grant/Award Number: PJT—178183

Abstract

Increased amplitude of peripheral vasomotion is a potential early marker of sepsis-related microcirculatory impairment; however, previous reports relied on clinically unsuitable invasive techniques. Hyperspectral near-infrared spectroscopy (hsNIRS) and diffuse correlation spectroscopy (DCS) are non-invasive, bedside techniques that can be paired to continuously monitor tissue hemoglobin content (HbT), oxygenation (StO₂), and perfusion (rBF) to detect vasomotion as low-frequency microhemodynamic oscillations. While previous studies have primarily focused on the peripheral microcirculation, cerebral injury is also a common occurrence in sepsis and hsNIRS-DCS could be used to assess cerebral microcirculatory function. This work aimed to use a hybrid hsNIRS-DCS system to continuously monitor changes in the peripheral and cerebral microcirculation in a rat model of early sepsis. It was hypothesized that the skeletal muscle would be a more sensitive early indicator of sepsis-related changes in microhemodynamics than the brain. Control animals received saline while the experimental group received fecal slurry to induce sepsis. Subsequently, hsNIRS-DCS measurements were acquired from the skeletal muscle and brain for 6 h. Peripheral rBF rapidly decreased in septic animals, but there were no significant changes in peripheral HbT or StO₂, nor cerebral HbT, rBF, or StO₂. The power of low-frequency

Abbreviations: $A(\lambda, t)$, attenuation spectrum; ABG, arterial blood gases; ANOVA, analysis of variance; BF_i, blood flow index; CWT, continuous wavelet transform; D_b , effective diffusion coefficient; DCS, diffuse correlation spectroscopy; DPF(λ), differential pathlength factor; Hb, deoxygenated hemoglobin; HbO, oxygenated hemoglobin; HbT, total hemoglobin; hsNIRS, hyperspectral near-infrared spectroscopy; $I_0(\lambda)$, reference light intensity; $I_{\text{dark}}(\lambda)$, background noise intensity; $I_{\text{tissue}}(\lambda)$, detected light intensity from tissue; ICU, intensive care unit; iNOS, inducible nitric oxide synthase; IP, intraperitoneal; IV, intravenous; IVVM, intravital video microscopy; K, correction factor for differential pathlength factor; MAP, mean arterial pressure; NA, numerical aperture; NIRS, near-infrared spectroscopy; NO, nitric oxide; Period 1, 0.5–2 h post injection; Period 2, 2.2–4 h post injection; Period 3, 4.2–6 h post injection; QQ, quantile–quantile; $R(\lambda)$, reflectance spectrum; RBC, red blood cells; rBF, relative blood flow; SPCM, single-photon counting module; StO₂, tissue oxygenation; t_0 , baseline period; VLS, visible-light spectroscopy; VSMCs, vascular smooth muscle cells; WF, water fraction; a , scatter amplitude; b , scatter power; α , proportion of moving scatterers; β , coherence factor; $\epsilon(\lambda)$, molar extinction coefficient; $G_1(\rho, \tau)$, electric field autocorrelation function; $g_2(\rho, \tau)$, normalized intensity autocorrelation; $\langle I \rangle$, average intensity; ρ , source-detector separation; $\mu_a(\lambda)$, absorption coefficient; $\mu_s'(\lambda)$, reduced scattering coefficient; τ , delay time.

This is an open access article under the terms of the [Creative Commons Attribution-NonCommercial](https://creativecommons.org/licenses/by-nc/4.0/) License, which permits use, distribution and reproduction in any medium, provided the original work is properly cited and is not used for commercial purposes.

© 2024 The Author(s). *The FASEB Journal* published by Wiley Periodicals LLC on behalf of Federation of American Societies for Experimental Biology.

peripheral oscillations in all parameters (i.e., HbT, StO₂, and rBF) as well as cerebral HbT oscillations were elevated in septic animals during the final 4 h. These findings suggest that in the early stages of sepsis, while vital organs like the brain are partly protected, changes in peripheral perfusion and vasomotor activity can be detected using hsNIRS-DCS. Future work will apply the technique to ICU patients.

KEYWORDS

diffuse correlation spectroscopy, microcirculatory impairment, near-infrared spectroscopy, sepsis, vasomotion

1 | INTRODUCTION

Sepsis, a dysregulated host response to infection that can result in life-threatening organ failure, is a leading global health burden that disproportionately affects vulnerable and low-resource populations.¹ Early administration of antibiotics and vasopressors to manage the infection and systemic hypotension, respectively, is associated with increased survival rate^{2,3}; however, there is currently a paucity of tools that are sensitive to the onset of sepsis to recognize the condition and triage patients for early intervention. Thus, there is a global need for accessible technology (i.e., non-invasive, preferably frugal, point-of-care) to guide early sepsis identification and intervention.

In the early stages of sepsis, the peripheral microcirculation becomes impaired.⁴⁻⁷ However, current clinical methods for quantifying microcirculatory function and perfusion in the clinic (e.g., capillary refill time, blood lactate, reactive hyperemia)⁸⁻¹⁰ are limited in their ability to continuously assess functional changes in specific microvascular beds. Near-infrared spectroscopy (NIRS) has been proposed as a non-invasive, bedside tool for continuous assessment of the peripheral and cerebral microcirculation in the intensive care unit (ICU).^{11,12} Current commercial NIRS systems typically utilize 2–4 wavelengths of near-infrared light to measure relative changes in the concentrations of oxygenated and deoxygenated hemoglobin (HbO and Hb, respectively) to quantify tissue oxygenation (StO₂), which reflects the oxygen supply–consumption balance in the microvasculature.¹³⁻¹⁵ While these approaches have demonstrated the practicality of NIRS for bedside monitoring in the ICU, they have not been sensitive to the functional deterioration of peripheral microcirculation in septic patients.¹⁶ A possible cause of this failure is that most of these studies make assumptions about total hemoglobin content (HbT) and optical pathlength in tissue,¹¹ which may not be valid with the expected changes in perfusion,¹⁷ blood volume,¹⁸ and circulation of peripheral immune cells during sepsis.¹⁹ These limitations could be addressed with the use of hyperspectral NIRS (hsNIRS),

which can simultaneously measure light absorption at hundreds of wavelengths, thereby enabling estimation of optical pathlength and absolute HbO, Hb, and HbT.²⁰⁻²⁵

Furthermore, NIRS biomarkers are commonly used to indirectly draw conclusions on microvascular perfusion.^{18,26} Autoregulatory mechanisms controlling arteriolar activity, however, may vary with the stage of sepsis²⁶; consequently, the degree of correlation between NIRS biomarkers and perfusion may be altered.^{23,27} To mitigate this limitation, a derivative of NIRS technology—namely, diffuse correlation spectroscopy (DCS)—can be used to directly quantify changes in microvascular blood flow in deep tissue by monitoring the dynamics of light scatterers, since these are primarily red blood cells (RBC).^{24,25,28,29} Interestingly, to monitor the microcirculation, hsNIRS and DCS can be paired for simultaneous measurements of hemoglobin, StO₂, and blood flow.^{23-25,30-33}

Recently, monitoring hemodynamic oscillations arising from fluctuations in vascular tone related to the heartbeat, respiration, and microvascular events has been suggested for assessing microcirculatory function.^{4,34} Notably, using intravital video microscopy (IVVM) on the exposed extensor digitorum longus muscle of rats, increased amplitude of low-frequency HbT oscillations has been shown to be sensitive to peripheral microcirculatory impairment in early sepsis.⁴ This phenotype is associated with increased amplitude of vasomotion—that is, low-frequency oscillations in vascular tone independent of faster hemodynamic oscillations related to the convective transport of oxygen by lung muscles and the heart.^{35,36} Vasomotion is affected by local events acting directly on the vasculature, such as endothelial, neurogenic, and myogenic activity,³⁴ and it is believed to play a regulatory role in tissue perfusion and oxygen delivery.^{35,37} While IVVM has provided valuable insights into microcirculatory vasomotion in early sepsis, it is an invasive technique that is unsuitable for clinical application. In contrast, hsNIRS and DCS can provide non-invasive in vivo measurements of skeletal muscle microcirculation³⁸; however, since these approaches detect a composite signal of all microhemodynamic events

affecting photon propagation within the tissue volume, their suitability for detecting sepsis-related vasomotion is unclear. Interestingly, continuous wavelet transform (CWT) can be applied to hsNIRS and DCS to decompose their signals into 2D time-frequency space to extract the amplitude of vasomotion as the power of low-frequency, tissue-level microhemodynamic oscillations.^{39–42}

Moreover, while previous work has primarily focused on changes in the peripheral microcirculation, brain injury is also a common short- and long-term complication of sepsis, with cerebral ischemia and microvascular injury suspected to be major contributors.^{43,44} Since, hsNIRS-DCS can monitor cerebral microcirculatory function, the technology could be used to detect early signs of cerebral injury. Nevertheless, the relative sensitivity of sepsis-related microcirculatory changes measurable with optical spectroscopy from the peripheral versus cerebral microcirculation is currently not well understood.

The objective of this study was to continuously monitor peripheral and cerebral microcirculation in a rat model of fecal-induced peritonitis, which has been previously demonstrated to provide a 6-h window between infection and clinical manifestation of sepsis.⁴ Changes in microvascular hemoglobin content, perfusion, oxygenation, and vasomotion were monitored from the skeletal muscle and brain using a hybrid hsNIRS-DCS system paired with CWT. It was hypothesized that the optical system could detect signs of sepsis-related microcirculatory impairment in the skeletal muscle earlier than in the brain.

2 | MATERIALS AND METHODS

2.1 | Animal model

All procedures were approved by Western University's Animal Care Committee (Protocol # 2019-053) and complied with guidelines established by the Canadian Council on Animal Care and Animal Research: Reporting of In Vivo Experiments. Initial sample size was determined according to a statistical power of 0.8 considering previous work with the same sepsis model.⁴ Based on preliminary findings of this study, the sample size was further increased to enable comparisons between sexes. Fourteen Sprague–Dawley rats (Charles River Laboratories, MA, USA), equally divided into male (weight: 300.1 ± 10.5 g) and female (weight: 245.3 ± 12.6 g), were procured and communally housed as same-sex pairs for 1 week prior to experimentation, reaching an age of 7–9 weeks at time of use. One animal from each of the first four pairs of rats was randomly assigned to the control group ($n=4$); the other half, along with the final six rats, constituted the experimental group ($n=10$).

The animals were anesthetized with sodium pentobarbital (65 mg/kg) and placed on a heat mat while being monitored with a rectal temperature probe to maintain core body temperature at $37 \pm 0.5^\circ\text{C}$. The left common carotid artery was cannulated to monitor mean arterial pressure (MAP) and draw blood samples. The right jugular vein was cannulated for intravenous (IV) fluid delivery. Animals were intubated after tracheostomy, and sufficient ventilation was confirmed through periodic measurements of arterial blood gases (ABG) and lactate using the VetScan i-STAT1 (Abbott Laboratories, IL, USA). Rats in the control group received an intraperitoneal (IP) injection of saline (0.9% NaCl administered at a dose of 3 mL/kg), while animals in the experimental group received an IP injection of fecal slurry (1 g of autologous feces per 1 mL of saline administered at a dose of 3 mL/kg) to induce sepsis.⁴ All animals received a constant infusion of saline at a rate of 0.5 mL per hour, which was increased to 6 mL per hour if MAP decreased below 65 mmHg. Pentobarbital maintenance boluses (up to 22 mg/kg) were administered as necessary through assessment of palpebral reflex and MAP.

2.2 | Instrumentation

An in-house built hybrid hsNIRS-DCS system was used to simultaneously probe the brain and skeletal muscle. Following surgical procedures, the scalp and hind limb were shaved, and identical probe holders were secured on the bald regions of interest for paired emission-detection of both optical modalities at a source-detector separation (ρ) of 10 mm (Figure 1).

The emission probes of the hsNIRS subsystem consisted of two identical multimode fibers (outer diameter = 2.5 mm, core = 800 μm , numerical aperture (NA) = 0.39; Thorlabs, NJ, USA) which directed light from two 20-W broadband halogen lamps (Ocean Insight, FL, USA) to the scalp and hind limb. A second pair of identical multimode fibers (outer diameter = 2.5 mm, core = 200 μm , NA = 0.39; Thorlabs) directed the diffusely reflected light from the two tissues to a QE Pro spectrometer (Ocean Insight) for brain monitoring and a QE 65000 spectrometer (Ocean Insight) for muscle monitoring.

The emission probe of the DCS subsystem consisted of a bifurcated multimode fiber (outer diameter = 2.5 mm, core = 400 μm , NA = 0.22; Thorlabs) which directed light from a 785-nm long-coherence-length laser (CrystaLaser, NV, USA) to the two tissues. Two identical fibers (few-mode at 785 nm, core = 8 μm , NA = 0.14; Thorlabs) directed the diffusely reflected laser light to two channels of a four-channel single-photon counting module (SPCM-AQ4C; Excelitas Technologies Corp., QC, Canada).

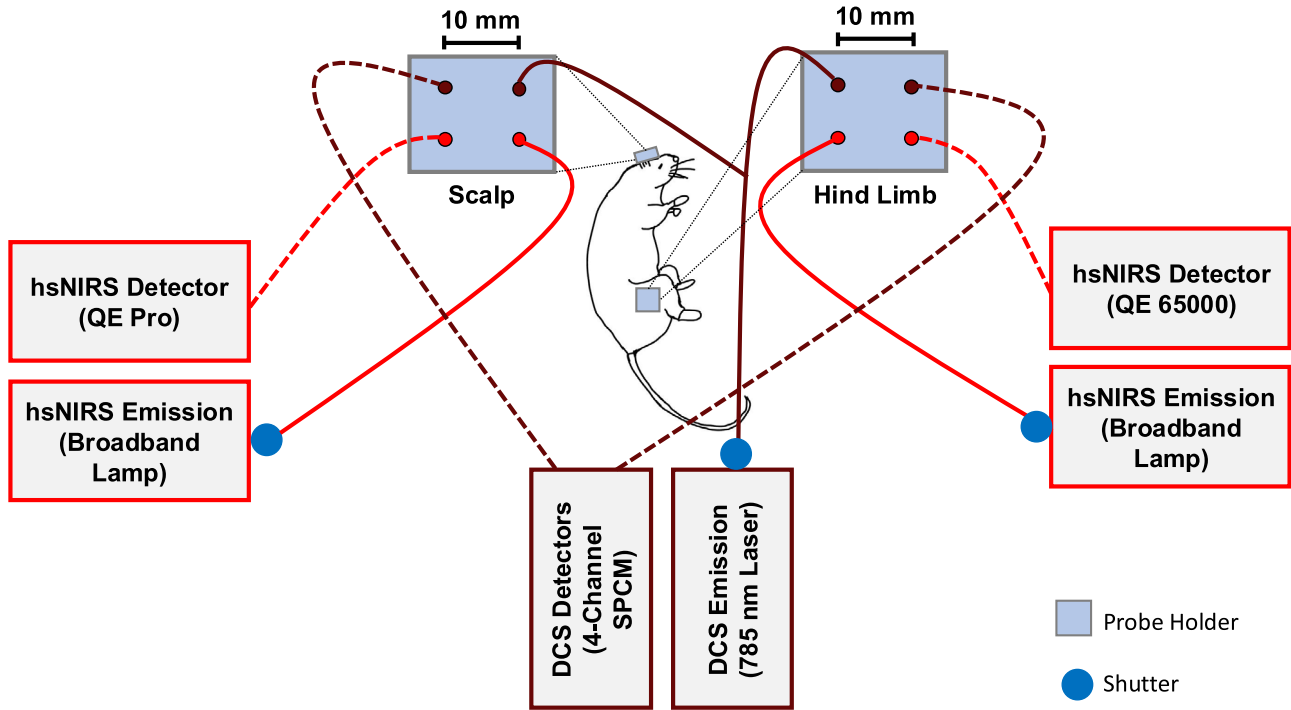


FIGURE 1 Simplified schematic (not drawn to scale) of the hybrid hsNIRS-DCS system. Emission fibers (solid lines) and detection fibers (dashed lines) are connected to magnified representations of the probe holders secured on the scalp and hind limb of the animals.

Prior to each experiment, the spectrum of a neon lamp and the reference light source (I_0) were acquired for wavelength and intensity calibration, respectively. To account for background light (I_{dark}) in the experimental environment, dark measurements were taken for reference, and tissue acquisitions by turning off the emission source. Further, to avoid crosstalk between the two optical modalities during the in vivo measurements, a shutter-based multiplexing system was used to alternately illuminate the tissues with the hsNIRS or DCS light source. In vivo measurements, with a sampling rate of 1 Hz, were taken simultaneously from the scalp and hind limb from 0.5–2 h (period 1), 2.2–4 h (period 2), and 4.2–6 h (period 3) post injection of saline or fecal slurry. ABG and lactate were measured within the first 30 min, and promptly after each period.

2.3 | Data processing

2.3.1 | Quantifying HbT and StO₂ from hsNIRS measurements

Using the reference, $I_0(\lambda)$, and dark signal spectra, tissue measurements at baseline were corrected to account for the intrinsic spectral property of the instrument, to obtain a reflectance spectrum (R):

$$R(\lambda) = \frac{I_{\text{tissue}}(\lambda) - I_{\text{dark}}(\lambda)}{I_0(\lambda) - I_{\text{dark}}(\lambda)} \quad (1)$$

Assuming that the main tissue chromophores in the near-infrared region (i.e., 680–850 nm) are Hb, HbO, and water (WF), absolute absorption and reduced scattering coefficients (μ_a and μ_s' , respectively) were subsequently quantified by fitting the first and second spectral derivatives of $\log[R(\lambda)]$ to the spectral derivatives of an analytical model based on a solution to the diffusion approximation for a semi-infinite homogenous medium^{21–25}:

$$\mu_a(\lambda) = \text{WF} \cdot \epsilon_{\text{H}_2\text{O}}(\lambda) + \text{Hb} \cdot \epsilon_{\text{Hb}}(\lambda) + \text{HbO} \cdot \epsilon_{\text{HbO}}(\lambda) \quad (2)$$

$$\mu_s'(\lambda) = a \left(\frac{\lambda}{800} \right)^{-b} \quad (3)$$

where ϵ_i (Equation 2) is the molar extinction coefficient of each chromophore, while a and b (Equation 3) characterize the overall scattering amplitude and power, respectively.

Subsequently, the differential pathlength factor (DPF), which is the ratio of mean pathlength traveled by light in tissue to ρ , was calculated from baseline μ_a and μ_s' and rescaled using a correction factor (K) determined by fitting the second derivative of $\log[R(\lambda)]$ to the second derivative of the known water absorption spectrum^{20,25,45,46}:

$$\text{DPF}(\lambda) = K \left(\frac{1}{2} \left(\frac{3\mu_s'(\lambda)}{\mu_a(\lambda)} \right)^{\frac{1}{2}} \left(1 - \frac{1}{1 + \rho(3\mu_a(\lambda)\mu_s'(\lambda))^{\frac{1}{2}}} \right) \right) \quad (4)$$

Following the estimation of the absolute baseline values, changes in chromophore concentrations (Δ Hb and

ΔHbO) were quantified with the modified Beer–Lambert Law from the measured changes in the broadband attenuation spectra (ΔA)^{23,25}:

$$\Delta A(\lambda, t) = \rho \cdot \text{DPF}(\lambda) \cdot (\Delta \text{Hb}(t) \cdot \varepsilon_{\text{Hb}}(\lambda) + \Delta \text{HbO}(t) \cdot \varepsilon_{\text{HbO}}(\lambda)) \quad (5)$$

HbT was calculated as the sum of Hb and HbO and StO_2 was quantified as follows:

$$\text{StO}_2(t) = 100\% \cdot \frac{\text{HbO}(t)}{\text{HbT}(t)} \quad (6)$$

2.3.2 | Quantifying rBF from DCS measurements

The electric field autocorrelation function (G_1) of brain and skeletal muscle were quantified from DCS measurements of normalized intensity autocorrelation (g_2) using the Siegert relation^{28,47,48}:

$$g_2(\rho, \tau) = 1 + \beta \frac{|G_1(\rho, \tau)|^2}{\langle I(\rho, \tau) \rangle^2} \quad (7)$$

where τ is the delay time, β is the coherence factor, and $\langle I \rangle$ is the average detected intensity. By incorporating time-varying μ_a and baseline μ_s' at 785 nm from hsNIRS analysis, the product of the proportion of moving scatterers (α) and effective diffusion coefficient (D_B) were obtained by fitting the data to a theoretical model of the correlation diffusion equation for a semi-infinite homogenous medium,

assuming a pseudo-Brownian motion.^{28,49} The product αD_B (in cm^2/s), representing blood flow index (BF_i), was used to estimate relative blood flow (rBF) as a percentage of baseline (t_0)⁴⁷:

$$\text{rBF}(t) = 100\% \cdot \frac{\text{BF}_i(t)}{\text{BF}_i(t_0)} \quad (8)$$

2.3.3 | Isolating microvascular oscillations using CWT

Upon quantification of HbT, StO_2 , and rBF time courses, CWT based on the Morlet wavelet was used to decompose the signal of each hemodynamic parameter into its frequency components (Figure 2).

While microvascular oscillations independent of cardiac, respiratory, and metabolic events are expected to affect hemodynamic parameters at frequencies of 0.0095–0.16 Hz in adult ICU patients,³⁴ the specific frequency band of pronounced vasomotion in this rat model of sepsis was identified as 0.02–0.06 Hz based on previous work,⁴ as well as visual inspection of septic versus control CWT in this study (Figure 3).

2.3.4 | Statistics

Normality was confirmed for all data prior to further statistical analysis through visual inspection of a

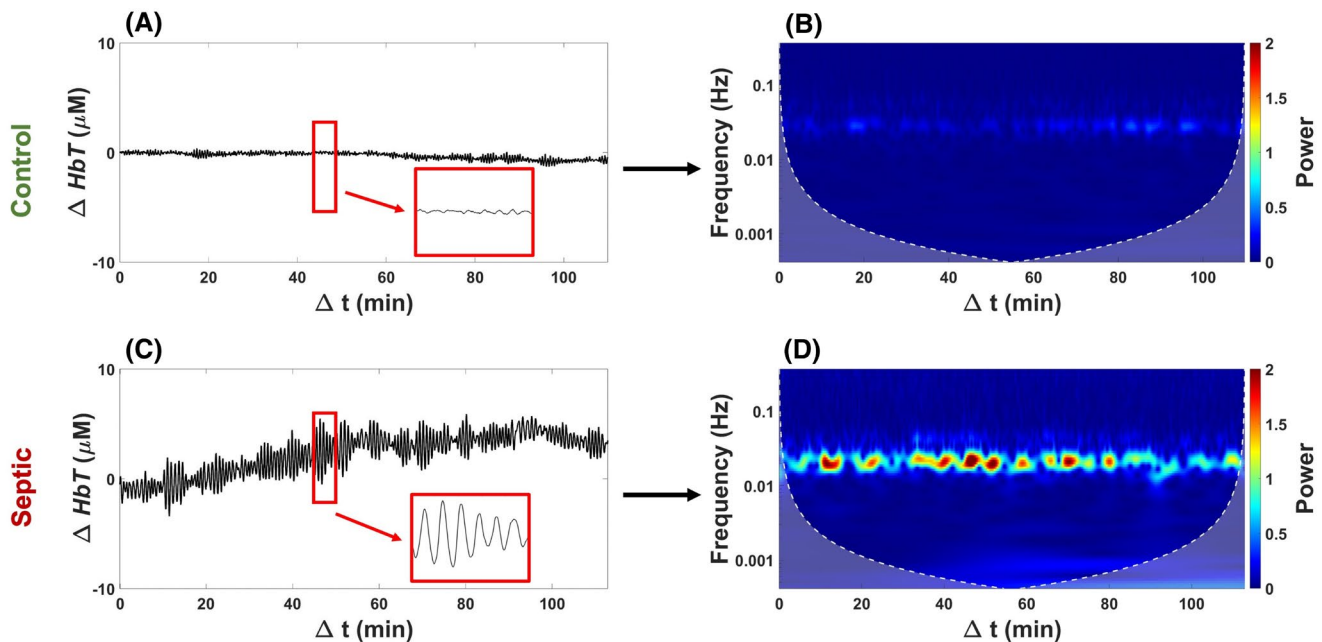


FIGURE 2 Sample ΔHbT time course of a control (A) and a septic rat (C), as well as heat maps corresponding to their CWT (B, D). For better visualization of vasomotion, 5 min within each time course is magnified in the red box. Cone of influence (dashed enclosure) delineates areas in the heat map that are potentially distorted by edge effects.

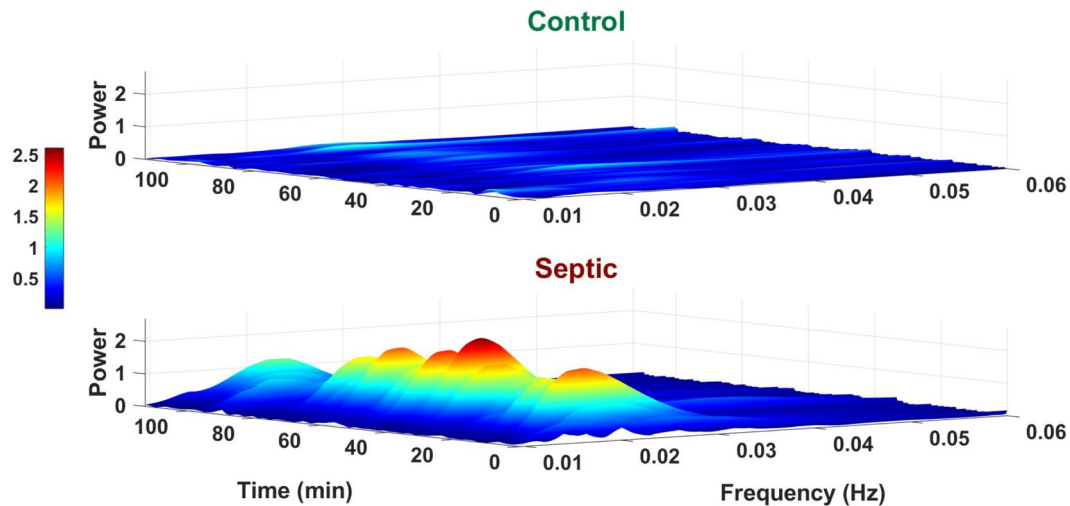


FIGURE 3 Sample 3D representation of septic versus control CWT of Δ HbT signal.

quantile–quantile (QQ) plot. Bonferroni correction was applied to all two-way analyses of variance (ANOVA), and $p < .05$ was considered significant.

For rBF, 5-min averages at the end of each period were computed and compared using a two-way ANOVA considering condition (control, septic) and time (period 1, period 2, period 3). Sex differences were investigated with a two-way ANOVA considering sex (septic male, septic female) and time. Lactate, MAP, HbT, and StO₂ at the start of period 1 and at the end of each period were also compared using multiple two-way ANOVAs to test for differences across condition, time, and sex.

Power of vasomotion in the skeletal muscle and brain of control and septic animals was quantified by first obtaining the maximum power in the vasomotion frequency range (0.02–0.06 Hz) across time from each hemodynamic parameter's CWT. Next, the median of the maximum power across each period was quantified and compared between animals using multiple two-way ANOVAs to test for differences across condition, time, sex, and tissue (skeletal muscle, brain).

All data and statistical analyses were performed on MATLAB R2022B (MathWorks, MA, USA) and Prism 10 (GraphPad Software Inc., MA, USA), respectively.

3 | RESULTS

In addition to the 14 animals included in the study, two were excluded: the first animal of the study (control male) was excluded due to signal disruptions from probe movements and software issues that compromised data acquisition. The first female animal (control) was excluded due

to an anesthetic dosing mistake which caused an early, irreversible hypotension.

Septic animals had elevated MAP compared to controls after 0.5 and 2 h (Figure 4A), which decreased significantly to lower than control by the end of 6 h. Sex differences in MAP were observed only at the end of 4 h, with septic females exhibiting a lower value. MAP continuously declined at all timepoints in septic animals (Figure 4A), dropping below 65 mmHg to prompt an increased rate of saline infusion in all five female septic rats after 4.7 ± 0.4 h and three of five septic males after 5.1 ± 0.4 h. Lactate was higher at all timepoints in septic animals (Figure 4B) but decreased from hours 2 to 4. Subsequently, lactate increased again from hours 4 to 6 in septic animals. No sex differences were observed in the lactate response.

Four samples of minute-by-minute timelapse videos of hemodynamic responses are provided in Supplemental Material to illustrate the typical peripheral and cerebral responses to saline and fecal slurry as captured by the hsNIRS-DCS system. Further, a table with the mean and standard deviation of all the results is provided in the Appendix 1.

3.1 | Peripheral perfusion and oxygenation changes

There were no differences in skeletal muscle HbT or StO₂ across condition, time, or sex (Figure 5A,B). Skeletal muscle rBF was lower in septic animals (Figure 5C) at the end of hours 2, 4, and 6. A decrease in rBF of septic skeletal muscle was observed from hours 2 to 4 which

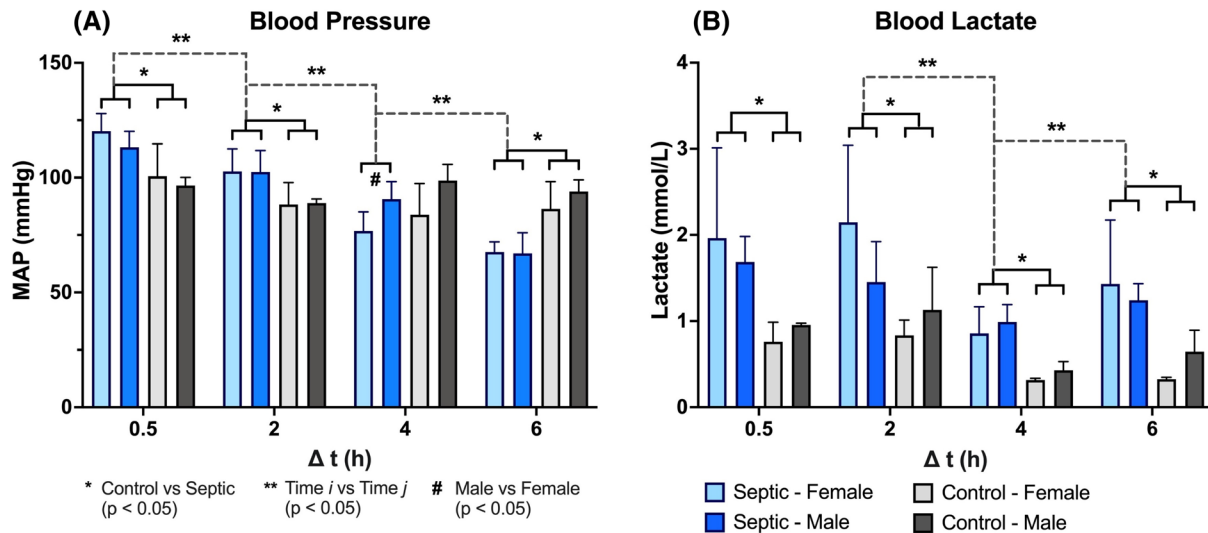


FIGURE 4 MAP (A) and blood lactate (B). Single asterisk indicates significant difference (two-way ANOVA with Bonferroni correction considering condition and time; $p < .05$) between septic ($n = 10$) and control ($n = 4$) animals, while double asterisks indicate significant difference across time. Hashtag indicates significant difference (two-way ANOVA with Bonferroni correction considering sex and time; $p < .05$) between male ($n = 5$) and female ($n = 5$) septic animals.

did not further decrease by the end of hour 6. At the 2-h mark, rBF in female septic animals was lower than male septic animals.

3.2 | Cerebral perfusion and oxygenation changes

No significant differences were observed between septic and control brain HbT, StO₂, or rBF (Figure 6A–C). However, a decrease was observed in septic animals from hours 2 to 4 in rBF and hours 0.5 to 2 in StO₂. There were no sex differences in cerebral HbT, StO₂, or rBF.

3.3 | Amplitude of peripheral vasomotion

The power of oscillations in the vasomotion frequency band was higher in periods 2 and 3 as reflected in all hemodynamic parameters (Figure 7A–C) measured from the skeletal muscle of septic animals in comparison to control animals. Furthermore, the power of vasomotion in all parameters increased with time from periods 1 to 2 and periods 2 to 3 in the septic animals.

Sex differences in septic animals were observed in the power of vasomotion reflected in StO₂ oscillations during the first period (Figure 7B), with males showing a higher power. In addition, septic males displayed a greater power of vasomotion reflected in rBF (Figure 7C) during period 2 and period 3.

3.4 | Amplitude of cerebral vasomotion

The power of cerebral vasomotion was greater in septic animals than control animals only in the HbT signal (Figure 8A) during period 2 and period 3, with septic males displaying a greater power in the first and final periods. The power of HbT oscillations increased from each period to the next. While not significantly different from controls, power of cerebral StO₂ oscillations (Figure 8B) increased from period 1 to 2 in septic animals. No differences were observed across condition, time, or sex in cerebral rBF oscillations (Figure 8C).

3.5 | Peripheral versus cerebral vasomotion

The power of peripheral oscillations was greater than the power of cerebral oscillations during all periods, as reflected in the HbT and rBF signals (Figure 9A,C). Further, the power of peripheral StO₂ oscillations (Figure 9B) was greater than the power of cerebral StO₂ oscillations during all periods past period 1.

4 | DISCUSSION

In this study, we assessed the ability of a non-invasive optical spectroscopy technique to detect microcirculatory changes before the onset of sepsis in a rat model of fecal-induced peritonitis through quantification of

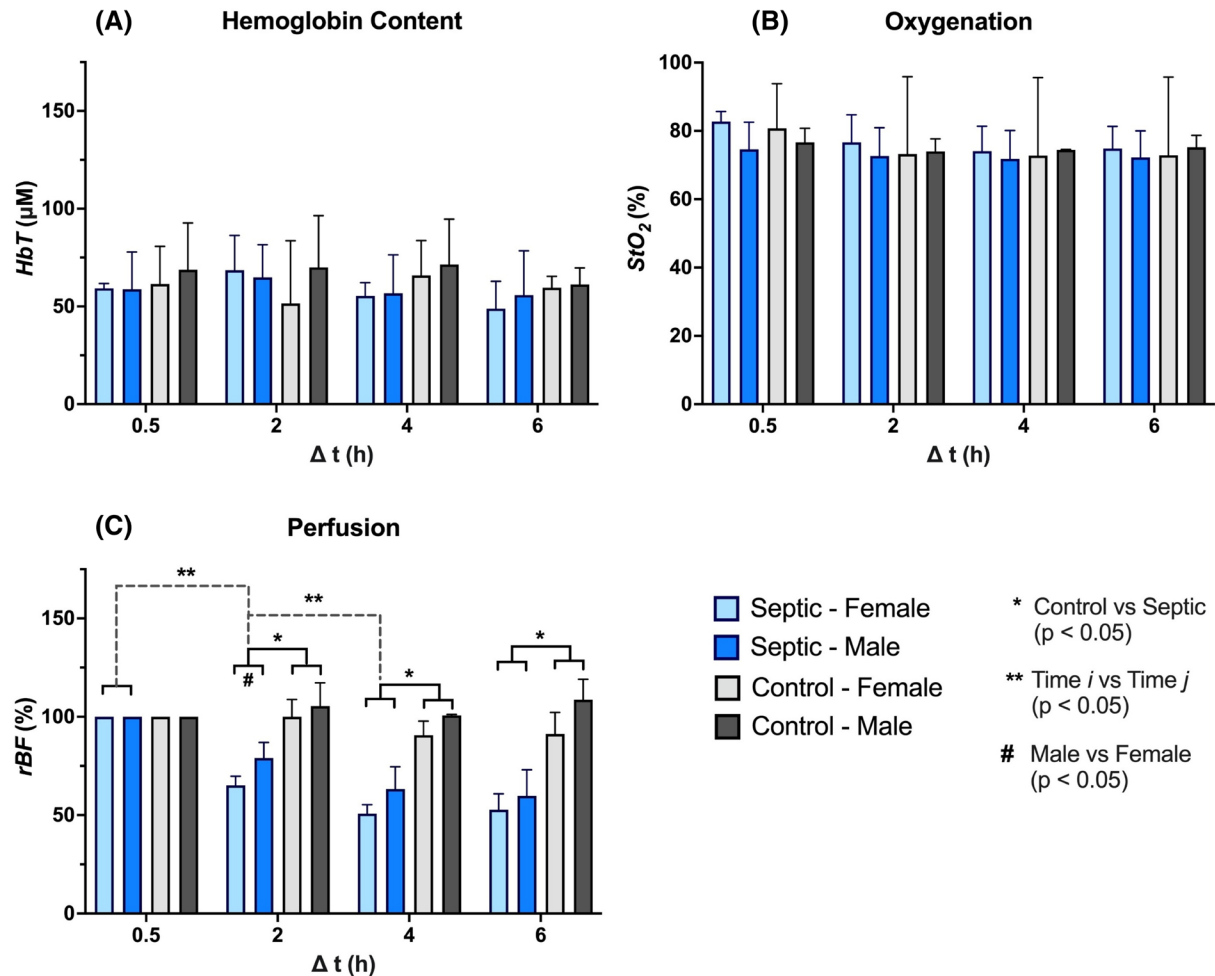


FIGURE 5 Peripheral HbT (A), StO_2 (B), and rBF (C). Single asterisk indicates significant difference (two-way ANOVA with Bonferroni correction considering condition and time; $p < .05$) between septic ($n = 10$) and control ($n = 4$) animals, while double asterisks indicate significant difference across time. Hashtag indicates significant difference (two-way ANOVA with Bonferroni correction considering sex and time; $p < .05$) between male ($n = 5$) and female ($n = 5$) septic animals.

peripheral and cerebral hemoglobin content, perfusion, oxygenation, and vasomotion. Measurements obtained with the hybrid hsNIRS-DCS system revealed that increased peripheral vasomotion could be an early marker of sepsis, which was in direct agreement with previous work using intravital video microscopy.⁴ Irreversible hypotension, which indicates progression toward septic shock and defined in this study as a MAP lower than 65 mmHg that cannot be resuscitated with increased saline infusion, was observed in 80% of septic animals within the third period. Interestingly, increased vasomotion was detected in the oscillations of all peripheral microhemodynamic parameters (i.e., HbT, StO_2 , rBF), as well as the oscillations of cerebral HbT, within the second period—that is, approximately 2 h before irreversible hypotension. Since blood flow resistance in the skeletal muscle substantially contributes to MAP, and considering the strong vasomotion detected in the muscle of the septic animals, power analysis was also

applied to MAP; however, no differences were observed across condition, time, or sex. The lack of a measurable impact from skeletal muscle vasomotion on MAP oscillations is likely because the former was not synchronous across different muscles.

Moreover, while skeletal muscle perfusion decreased significantly in septic animals, no changes were observed in peripheral hemoglobin content or oxygenation, nor cerebral hemoglobin, oxygenation, or perfusion; however, the study was likely underpowered to detect a statistically significant difference in cerebral perfusion, which strongly correlated with MAP. In agreement with the peripheral hypoperfusion detected with DCS, blood lactate was elevated in septic animals throughout the 6 h.¹⁷ The early decrease in skeletal muscle perfusion was greater in female septic animals than males, and all females experienced irreversible hypotension, as opposed to three of five males. Further, while females exhibited a more rapid progression toward hypotension, peripheral and cerebral vasomotion

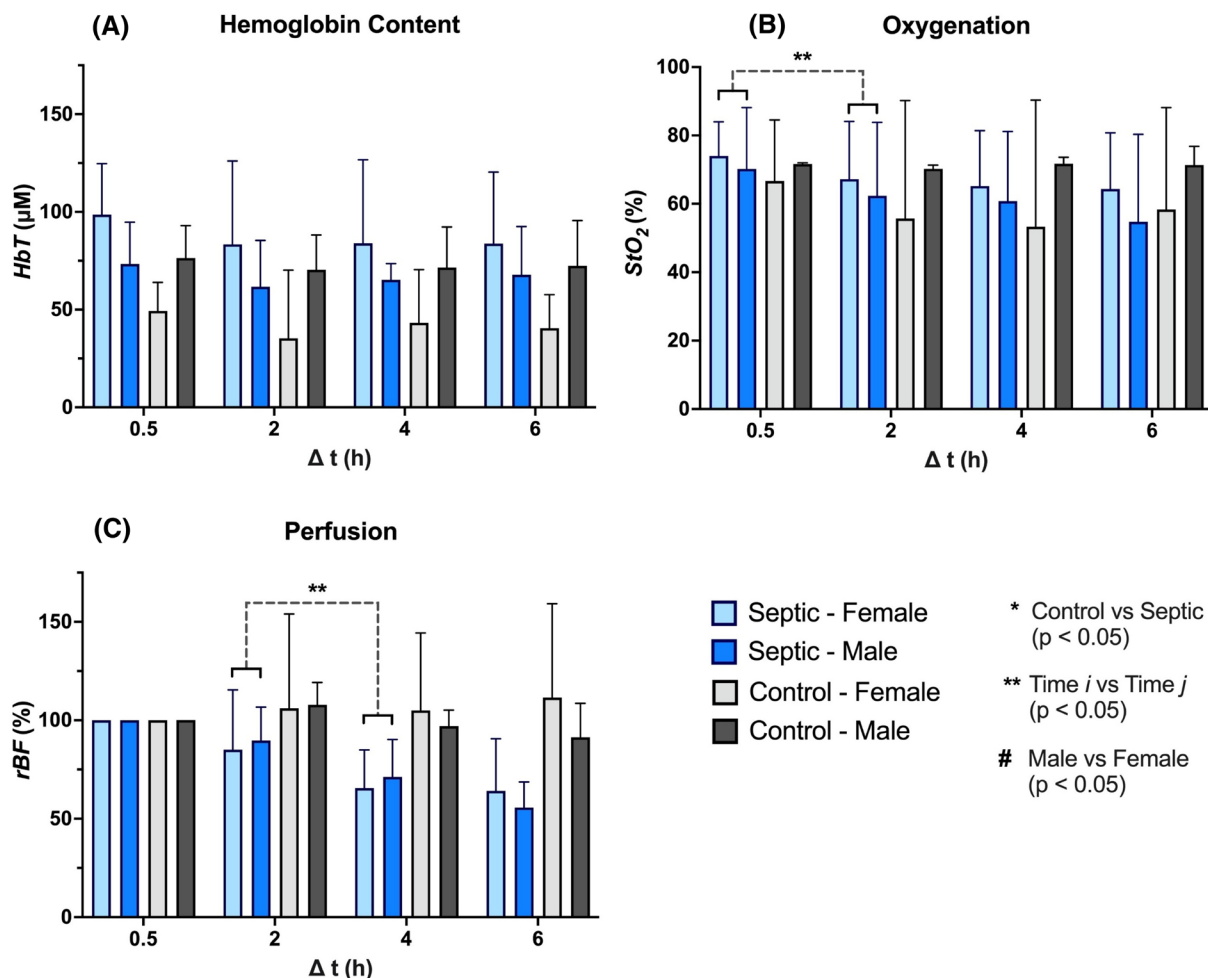


FIGURE 6 Cerebral HbT (A), StO_2 (B), and rBF (C). Single asterisk indicates significant difference (two-way ANOVA with Bonferroni correction considering condition and time; $p < .05$) between septic ($n = 10$) and control ($n = 4$) animals, while double asterisks indicate significant difference across time. Hashtag indicates significant difference (two-way ANOVA with Bonferroni correction considering sex and time; $p < .05$) between male ($n = 5$) and female ($n = 5$) septic animals.

were higher in males. Importantly, in this model of early sepsis, the peripheral microvasculature probed through the hind limb was a more sensitive early target for detecting impairment than the cerebral microvasculature.

Furthermore, while some MAP-driven decreases were observed in cerebral perfusion, the DCS data revealed considerable skeletal muscle hypoperfusion independent of changes in MAP during the early response to infection—a probable hyperdynamic response to increase blood flow to vital organs.⁵⁰ This reaction likely begins with notable peripheral vasoconstriction to shunt blood, from which hypoxia in arteriolar vascular smooth muscle cells (VSMCs) may ensue considering the low average blood flow. When sufficiently hypoxic, VSMCs would be unable to maintain tone; with the expected increase in inducible nitric oxide synthase (iNOS) during sepsis and consequently nitric oxide (NO),⁵¹ a vasodilator acting on VSMCs, the arterioles would subsequently dilate, bringing in RBCs and restoring oxygen levels for constriction to reinitiate. Accordingly, the counter

cooperation of constriction and dilation would manifest as vasomotion with a pseudo-periodic pattern.

It is thought that increased amplitude of vasomotion may improve local oxygenation and perfusion.^{35,37,52} This could explain the finding of this study that in the final 2 h of the experiment, the amplitude of peripheral vasomotion continued to increase while the average value in skeletal muscle rBF stopped decreasing. Furthermore, males expressed a greater amplitude of peripheral vasomotion but experienced a smaller average decrease in skeletal muscle perfusion. Clearance of metabolic byproducts (e.g., lactate), the levels of which may vary with sex given the cardioprotective nature of estrogen that improves mitochondrial function,⁵³ may also contribute to vasomotion. Despite the sex-dependent differences in vasomotion, however, no differences were observed in blood lactate in this study.

Importantly, despite the decrease in peripheral rBF and increase in vasomotion in septic animals, the NIRS data did not suggest tissue hypoxia in the skeletal muscle

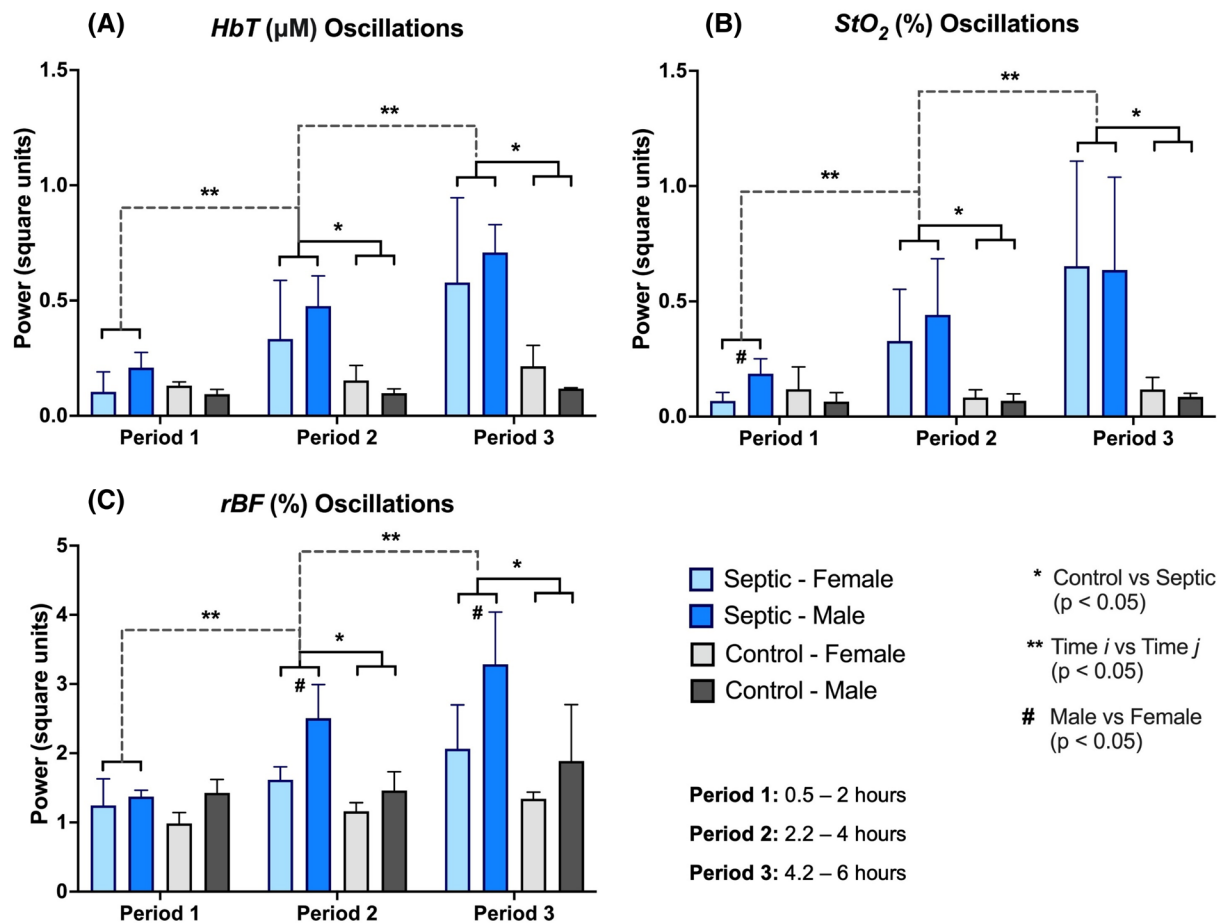


FIGURE 7 Power of peripheral vasomotion (0.02–0.06 Hz) reflected in HbT (A), StO₂ (B), and rBF (C) oscillations. Single asterisk indicates significant difference (two-way ANOVA with Bonferroni correction considering condition and time; $p < .05$) between septic ($n = 10$) and control ($n = 4$) animals, while double asterisks indicate significant difference across time. Hashtag indicates significant difference (two-way ANOVA with Bonferroni correction considering sex and time; $p < .05$) between male ($n = 5$) and female ($n = 5$) septic animals.

nor brain, thereby suggesting an impairment in the coupling of oxygen supply and regulation with tissue oxygen demand.⁴ A potential confounder in the peripheral microcirculation, however, is myoglobin, which has a nearly identical absorption spectrum to that of hemoglobin, thereby limiting accurate representations of StO₂ and potentially giving the illusion of adequate tissue oxygen saturation.

Structural plugging of capillaries by excess peripheral immune cells and microthrombi have been frequently suggested as the driving mechanisms for microcirculatory impairment in sepsis.^{54,55} However, previous work has repeatedly failed to validate this hypothesis,^{4,56,57} and increased peripheral vasomotion precedes increased stopped flow of RBC through capillaries,⁴ making plugging an insufficient explanation for this unstable phenotype. Since the fall in skeletal muscle blood flow was demonstrated to occur prior to increased vasomotion, the results of this study suggest that the deterioration of peripheral microvascular perfusion is also likely independent of capillary

plugging during sepsis. Alternatively, impaired endothelial conduction has been attributed to the diminished oxygen signaling from capillaries, where sensing of stimuli in active tissue takes place, to upstream arterioles and VSMCs.^{4,58–62}

4.1 | Increased amplitude of vasomotion reduces vascular resistance

While increased amplitude of vasomotion is associated with improved perfusion proximal to the arteriolar network,^{35,52} it is also paired with reduced vascular resistance.⁶³ Progressive systemic hypotension and non-responsiveness of vascular resistance to fluids are common in patients with septic shock.^{64,65} The results of this study suggest that the exaggerated peripheral vasomotion may contribute to the failure of the skeletal muscle arterioles in maintaining sufficient resistance and regulating MAP.^{60,63}

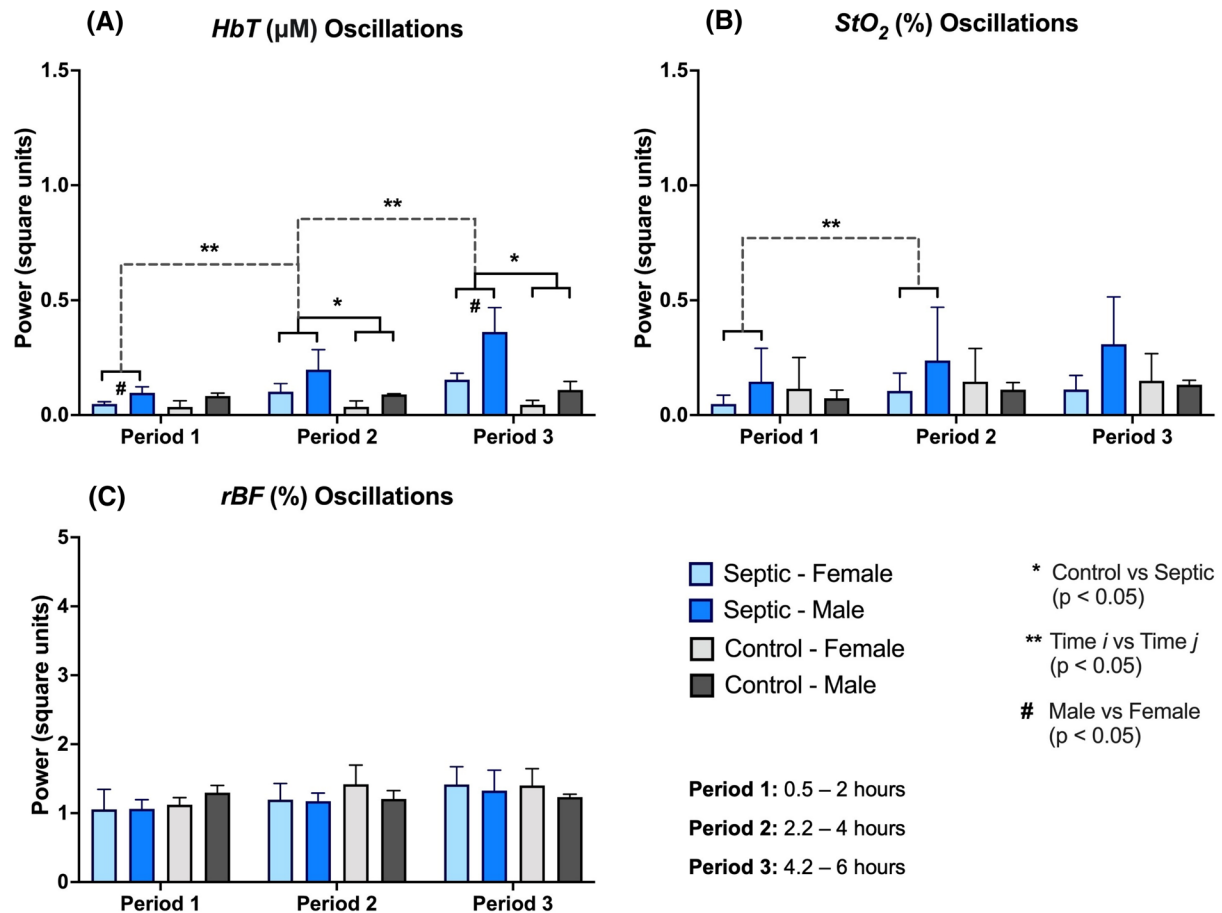


FIGURE 8 Power of cerebral vasomotion (0.02–0.06 Hz) reflected in HbT (A), StO₂ (B), and rBF (C) oscillations. Single asterisk indicates significant difference (two-way ANOVA with Bonferroni correction considering condition and time; $p < .05$) between septic ($n = 10$) and control ($n = 4$) animals, while double asterisks indicate significant difference across time. Hashtag indicates significant difference (two-way ANOVA with Bonferroni correction considering sex and time; $p < .05$) between male ($n = 5$) and female ($n = 5$) septic animals. The vertical axes are kept as Figure 7 for consistency and ease of visual comparison.

4.2 | Study limitations and future work

This study used a homogenous animal model without therapeutic intervention, which does not capture the clinical heterogeneity of hospitalized patients with sepsis. Future work that considers alternative modes of infection with longer monitoring periods, comorbidities like diabetes, as well as interventions like antibiotics and fluid boluses could better capture this diversity. Moreover, due to metabolic differences, males and females received different anesthetic maintenance doses.^{66,67} However, this was necessary to avoid premature hypotension in females. Further, interpretations of the changes to cerebral perfusion in this study were limited by the use of sodium pentobarbital, as this anesthetic disrupts cerebral autoregulation,⁶⁸ thereby harmonizing rBF changes with changes in MAP.

Future work using a contrast agent, such as Indocyanine green and IRDye carboxylate, could reveal differences in absolute blood flow and endothelial permeability (e.g.,

blood–brain barrier).⁶⁹ As well, assessment of the techniques used in this study for characterizing peripheral microcirculatory function in diverse ICU patients is needed before clinical translation.

4.3 | Conclusions

This study demonstrated the feasibility of using non-invasive optical spectroscopy to detect early onset of microcirculatory impairment during sepsis. Prior to changes in tissue oxygenation, as commonly monitored with commercial NIRS devices, decreased peripheral perfusion was measured with DCS, and increased vasomotion was detected by pairing NIRS or DCS with CWT. The results of this study suggest that while the brain is partly protected in early sepsis, the skeletal muscle could be an early target for detecting changes in microhemodynamics. Future work will assess the sensitivity of these techniques for monitoring changes

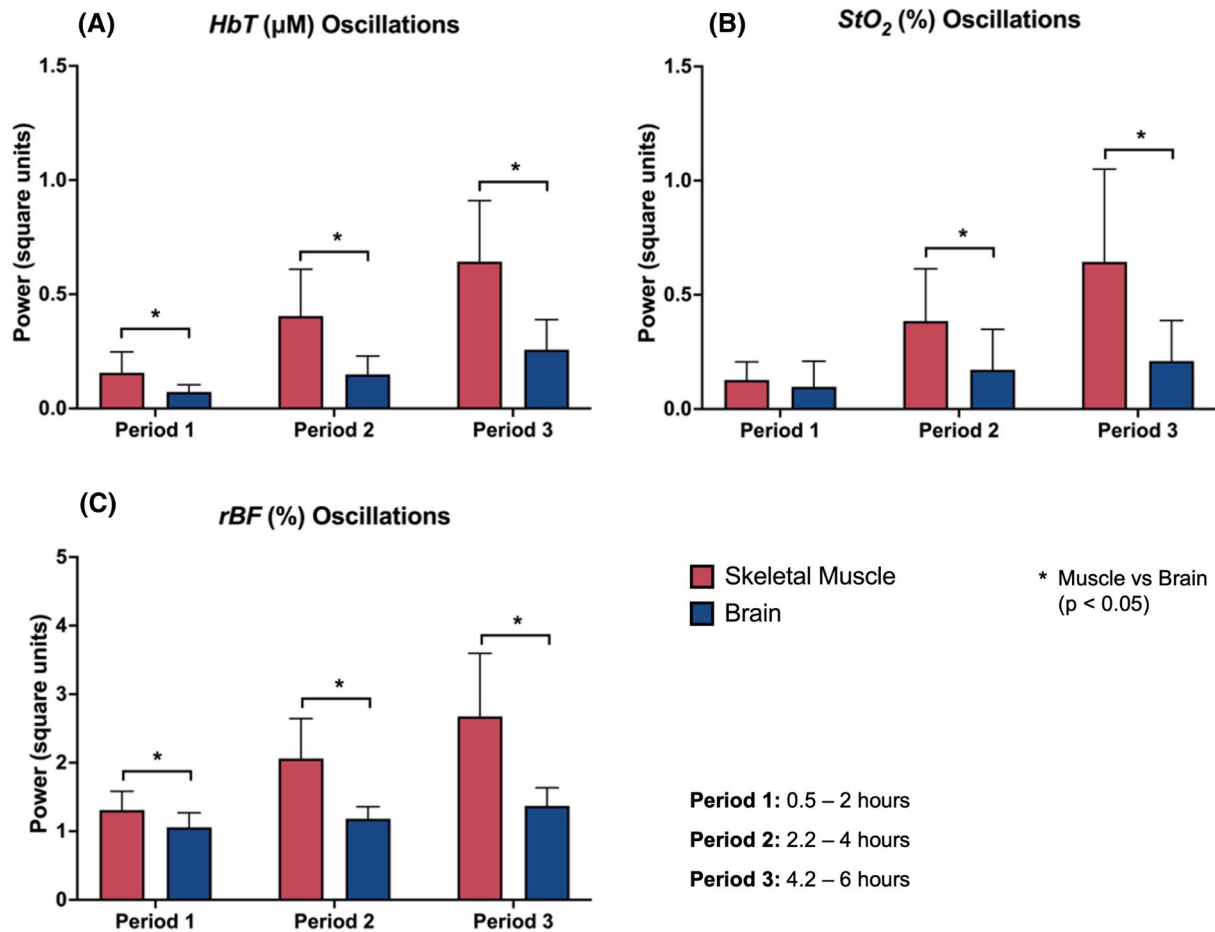


FIGURE 9 Power of peripheral versus cerebral vasomotion (0.02–0.06 Hz) reflected in HbT (A), StO₂ (B), and rBF (C) oscillations. Single asterisk indicates significant difference (two-way ANOVA with Bonferroni correction considering tissue and time; $p < .05$) between septic muscle ($n = 10$) and septic brain ($n = 10$).

in microcirculatory function of diverse septic and non-septic ICU patients.

AUTHOR CONTRIBUTIONS

Rasa Eskandari adapted the hybrid optical hsNIRS-DCS system to this study and collected experimental data, performed data and statistical analyses, interpreted results, and prepared the manuscript draft. Stephanie Milkovich performed all hands-on animal work. Farah Kamar, Dr. Daniel Goldman, and Dr. Donald G. Welsh contributed to results interpretation. Dr. Christopher G. Ellis contributed to study conception, design, and results interpretation. Dr. Mamadou Diop was the senior author and provided technical expertise, while contributing to study design and results interpretation. All authors edited the manuscript draft and approved the final version.

ACKNOWLEDGMENTS

We thank Dr. Daniel Milej for the development of the DCS data acquisition software and the shutter control software.

FUNDING INFORMATION

This study was supported by the Canadian Institutes of Health Research (PJT—178183) and a Queen Elizabeth II Graduate Scholarship in Science and Technology.

DISCLOSURES

The authors declare that they have no competing interests.

DATA AVAILABILITY STATEMENT

The data that supports the findings of this study is available from the corresponding author upon reasonable request.

ORCID

Rasa Eskandari <https://orcid.org/0009-0001-6702-9110>

Stephanie Milkovich <https://orcid.org/0009-0002-8813-2085>

Farah Kamar <https://orcid.org/0000-0001-5913-0721>

Daniel Goldman <https://orcid.org/0000-0002-8707-5536>

<https://orcid.org/0000-0002-8707-5536>

Donald G. Welsh  <https://orcid.org/0000-0001-5174-186X>

Christopher G. Ellis  <https://orcid.org/0000-0002-7760-1846>

Mamadou Diop  <https://orcid.org/0000-0003-1244-7830>

REFERENCES

- Rudd KE, Johnson SC, Agesa KM, et al. Global, regional, and national sepsis incidence and mortality, 1990–2017: analysis for the Global Burden of Disease Study. *Lancet* www.thelancet.com. 2020;395:200-211. doi:10.1016/S0140-6736(19)32989-7
- Il KH, Park S. Sepsis: early recognition and optimized treatment. *Tuberc Respir Dis (Seoul)*. 2019;82(1):6-14. doi:10.4046/trd.2018.0041
- Seymour CW, Gesten F, Prescott HC, et al. Time to treatment and mortality during mandated emergency care for sepsis. *New Engl J Med*. 2017;376(23):2235-2244. doi:10.1056/nejmoa1703058
- Kowalewska PM, Kowalewski JE, Milkovich SL, et al. Spectroscopy detects skeletal muscle microvascular dysfunction during onset of sepsis in a rat fecal peritonitis model. *Sci Rep*. 2022;12:6339. doi:10.1038/s41598-022-10208-w
- Davis JS, Yeo TW, Thomas JH, et al. Sepsis-associated microvascular dysfunction measured by peripheral arterial tonometry: an observational study. *Crit Care*. 2009;13(5):R155. doi:10.1186/cc8055
- Miranda M, Balarini M, Caixeta D, Bouskela E. Microcirculatory dysfunction in sepsis: pathophysiology, clinical monitoring, and potential therapies. *Am J Physiol-Heart Circulat Physiol*. 2016;311(1):H24-H35. doi:10.1152/ajpheart.00034.2016
- Ince C. The microcirculation is the motor of sepsis. *Crit Care*. 2005;9(suppl 4):S13-S19. doi:10.1186/cc3753
- Ait-Oufella H, Bige N, Boelle PY, et al. Capillary refill time exploration during septic shock. *Intensive Care Med*. 2014;40(7):958-964. doi:10.1007/s00134-014-3326-4
- de Menezes IAC, da Cunha CL, Junior HC, Luy AM. Increase of perfusion index during vascular occlusion test is paradoxically associated with higher mortality in septic shock after fluid resuscitation: a prospective study. *Shock*. 2019;51(5):605-612. doi:10.1097/SHK.0000000000001217
- Mayeur C, Campard S, Richard C, Teboul JL. Comparison of four different vascular occlusion tests for assessing reactive hyperemia using near-infrared spectroscopy. *Crit Care Med*. 2011;39(4):695-701. doi:10.1097/CCM.0b013e318206d256
- Skarda DE, Mulier KE, Myers DE, Taylor JH, Beilman GJ. Dynamic near-infrared spectroscopy measurements in patients with severe sepsis. *Shock*. 2007;27(4):348-353. doi:10.1097/01.shk.0000239779.25775.e4
- Shapiro NI, Arnold R, Sherwin R, et al. The association of near-infrared spectroscopy-derived tissue oxygenation measurements with sepsis syndromes, organ dysfunction and mortality in emergency department patients with sepsis. *Crit Care*. 2011;15(5):R223. doi:10.1186/cc10463
- Azuma K, Homma S, Kagaya A. Oxygen supply-consumption balance in the thigh muscles during exhausting knee-extension exercise. *J Biomed Opt*. 2000;5(1):97-101. doi:10.1117/1.429974
- Quaresima V, Lepanto R, Ferrari M. The use of near infrared spectroscopy in sports medicine. *J Sports Med Phys Fitness*. 2003;43(1):1-13. Accessed August 17, 2023. <https://europepmc.org/article/med/12629456>
- Lima A, Bakker J. Near-infrared spectroscopy for monitoring peripheral tissue perfusion in critically ill patients. *Rev Bras Ter Intensiva*. 2011;23(3):341-351. doi:10.1590/S0103-507X2011000300013
- Nardi O, Zavala E, Martin C, et al. Targeting skeletal muscle tissue oxygenation (StO₂) in adults with severe sepsis and septic shock: a randomised controlled trial (OTO-StS Study). *BMJ Open*. 2018;8(3):e017581. doi:10.1136/bmjopen-2017-017581
- Hernandez G, Pedreros C, Veas E, et al. Evolution of peripheral vs. metabolic perfusion parameters during septic shock resuscitation. A clinical-physiologic study. *J Crit Care*. 2012;27(3):283-288. doi:10.1016/j.jcrc.2011.05.024
- Girardis M, Rinaldi L, Busani S, Flore I, Mauro S, Pasetto A. Muscle perfusion and oxygen consumption by near-infrared spectroscopy in septic-shock and non-septic-shock patients. *Intensive Care Med*. 2003;29(7):1173-1176. doi:10.1007/s00134-003-1805-0
- Rimmelé T, Payen D, Cantaluppi V, et al. Immune cell phenotype and function in sepsis. *Shock*. 2016;45(3):282-291. doi:10.1097/SHK.0000000000000495
- Scholkmann F, Wolf M. General equation for the differential pathlength factor of the frontal human head depending on wavelength and age. *J Biomed Opt*. 2013;18(10):105004. doi:10.1117/1.JBO.18.10.105004
- Kewin M, Rajaram A, Milej D, et al. Evaluation of hyperspectral NIRS for quantitative measurements of tissue oxygen saturation by comparison to time-resolved NIRS. *Biomed. Opt Express*. 2019;10(9):4789-4802. doi:10.1364/BOE.10.004789
- Diop M, Toronov V, Lee TY, Lawrence KS, Yeganeh HZ, Elliott JT. Broadband continuous-wave technique to measure baseline values and changes in the tissue chromophore concentrations. *Biomed Opt Express*. 2012;3(11):2761-2770. doi:10.1364/BOE.3.002761
- Rajaram A, Milej D, Suwalski M, et al. Assessing cerebral blood flow, oxygenation and cytochrome c oxidase stability in preterm infants during the first 3 days after birth. *Sci Rep*. 2022;12:181. doi:10.1038/s41598-021-03830-7
- Diop M, Kishimoto J, Toronov V, Lee DS, St Lawrence K. Development of a combined broadband near-infrared and diffusion correlation system for monitoring cerebral blood flow and oxidative metabolism in preterm infants. *Biomed Opt Express*. 2015;6(10):3907-3918. doi:10.1364/BOE.6.003907
- Rajaram A, Bale G, Kewin M, et al. Simultaneous monitoring of cerebral perfusion and cytochrome c oxidase by combining broadband near-infrared spectroscopy and diffuse correlation spectroscopy. *Biomed Opt Express*. 2018;9(6):2588-2603. doi:10.1364/BOE.9.002588
- Wood MD, Boyd JG, Wood N, et al. The use of near-infrared spectroscopy and/or transcranial Doppler as non-invasive markers of cerebral perfusion in adult sepsis patients with delirium: a systematic review. *J Intensive Care Med*. 2022;37(3):408-422. doi:10.1177/0885066621997090
- Brady K, Joshi B, Zweifel C, et al. Real-time continuous monitoring of cerebral blood flow autoregulation using near-infrared spectroscopy in patients undergoing cardiopulmonary bypass. *Stroke*. 2010;41(9):1951-1956. doi:10.1161/STROKEAHA.109.575159

28. Durduran T, Yodh AG. Diffuse correlation spectroscopy for non-invasive, micro-vascular cerebral blood flow measurement. *NeuroImage*. 2013;85:51-63. doi:[10.1016/j.neuroimage.2013.06.017](https://doi.org/10.1016/j.neuroimage.2013.06.017)
29. Selb J, Wu KC, Sutin J, et al. Prolonged monitoring of cerebral blood flow and autoregulation with diffuse correlation spectroscopy in neurocritical care patients. *Neurophotonics*. 2018;5(4):1. doi:[10.1117/1.NPh.5.4.045005](https://doi.org/10.1117/1.NPh.5.4.045005)
30. Rajaram A, Yip LCM, Suwalski M, et al. NNeMo (Neonatal NeuroMonitor): a non-invasive brain monitor for continuous acquisition of cerebral blood flow and cytochrome c oxidase in the premature brain. In: Fantini S, Taroni P, eds. *Optical Tomography and Spectroscopy of Tissue XIV*. SPIE; 2021:40. doi:[10.1117/12.2578721](https://doi.org/10.1117/12.2578721)
31. Milej D, Rajaram A, Suwalski M, et al. Hybrid hsNIRS/DCS system for assessing cerebral blood flow and cytochrome c oxidase stability in preterm infants. *Biophotonics Congress: Biomedical Optics 2022 (Translational, Microscopy, OCT, OTS, BRAIN)*. Optica Publishing Group; 2022:BTu2C.4. doi:[10.1364/BRAIN.2022.BTu2C.4](https://doi.org/10.1364/BRAIN.2022.BTu2C.4)
32. Suwalski M, Shoemaker LN, Shoemaker JK, et al. Assessing the sensitivity of multi-distance hyperspectral NIRS to changes in the oxidation state of cytochrome C oxidase in the brain. *Metabolites*. 2022;12(9):817. doi:[10.3390/metabo12090817](https://doi.org/10.3390/metabo12090817)
33. Suwalski M, Milej D, Rajaram A, et al. Optical assessment of the response in cerebral metabolism to mean arterial pressure during the transition onto cardiopulmonary bypass. In: Lilge LD, Huang Z, eds. *Translational Biophotonics: Diagnostics and Therapeutics III*. SPIE; 2023:45. doi:[10.1117/12.2670594](https://doi.org/10.1117/12.2670594)
34. Mendelson AA, Rajaram A, Bainbridge D, et al. Dynamic tracking of microvascular hemoglobin content for continuous perfusion monitoring in the intensive care unit: pilot feasibility study On behalf of the Canadian Critical Care Translational Biology Group. *J Clin Monit Comput*. 2021;35(3):1453-1465. doi:[10.1007/s10877-020-00611-x](https://doi.org/10.1007/s10877-020-00611-x)
35. Nilsson H. Vasomotion: mechanisms and physiological importance. *Mol Interv*. 2003;3(2):79-89. doi:[10.1124/mi.3.2.79](https://doi.org/10.1124/mi.3.2.79)
36. Aalkjær C, Boedtker D, Matchkov V. Vasomotion—what is currently thought? *Acta Physiol*. 2011;202(3):253-269. doi:[10.1111/j.1748-1716.2011.02320.x](https://doi.org/10.1111/j.1748-1716.2011.02320.x)
37. Goldman D, Popel AS. A computational study of the effect of vasomotion on oxygen transport from capillary networks. *J Theor Biol*. 2001;209(2):189-199. doi:[10.1006/jtbi.2000.2254](https://doi.org/10.1006/jtbi.2000.2254)
38. Mawdsley L. *Using Hyperspectral Near-Infrared Spectroscopy and Diffuse Correlation Spectroscopy to Monitor the Effects of Phenylephrine in the Microcirculation*. Electronic Thesis and Dissertation Repository. 8294. Western University; 2021.
39. Stefanovska A, Bracic M, Kvernmo HD. Wavelet analysis of oscillations in the peripheral blood circulation measured by laser Doppler technique. *IEEE Trans Biomed Eng*. 1999;46(10):1230-1239. doi:[10.1109/10.790500](https://doi.org/10.1109/10.790500)
40. Kvandal P, Landsverk SA, Bernjak A, Stefanovska A, Kvernmo HD, Kirkeboen KA. Low-frequency oscillations of the laser Doppler perfusion signal in human skin. *Microvasc Res*. 2006;72(3):120-127. doi:[10.1016/j.mvr.2006.05.006](https://doi.org/10.1016/j.mvr.2006.05.006)
41. Bernjak A, Stefanovska A. Importance of wavelet analysis in laser Doppler flowmetry time series. 2007 *29th Annual International Conference of the IEEE Engineering in Medicine and Biology Society*. IEEE; 2007:4064-4067. doi:[10.1109/IEMBS.2007.4353226](https://doi.org/10.1109/IEMBS.2007.4353226)
42. Bernjak A, Clarkson PBM, McClintock PVE, Stefanovska A. Low-frequency blood flow oscillations in congestive heart failure and after β 1-blockade treatment. *Microvasc Res*. 2008;76(3):224-232. doi:[10.1016/j.mvr.2008.07.006](https://doi.org/10.1016/j.mvr.2008.07.006)
43. Taccone FS, Su F, Pierrakos C, et al. Cerebral microcirculation is impaired during sepsis: an experimental study. *Crit Care*. 2010;14(4):R140. doi:[10.1186/cc9205](https://doi.org/10.1186/cc9205)
44. Ehlenbach WJ, Sonnen JA, Montine TJ, Larson EB. Association between sepsis and microvascular brain injury. *Crit Care Med*. 2019;47(11):1531-1538. doi:[10.1097/CCM.0000000000003924](https://doi.org/10.1097/CCM.0000000000003924)
45. Matcher SJ, Cope M, Delpy DT. Use of the water absorption spectrum to quantify tissue chromophore concentration changes in near-infrared spectroscopy. *Phys Med Biol*. 1994;39(1):177-196. doi:[10.1088/0031-9155/39/1/011](https://doi.org/10.1088/0031-9155/39/1/011)
46. Mawdsley L, Eskandari R, Kamar F, et al. In vivo optical assessment of cerebral and skeletal muscle microvascular response to phenylephrine. *FASEB BioAdv*. 2024;6(9):390-399. doi:[10.1096/fba.2024-00063](https://doi.org/10.1096/fba.2024-00063)
47. Diop M, Verdecchia K, Lee TY, St Lawrence K. Calibration of diffuse correlation spectroscopy with a time-resolved near-infrared technique to yield absolute cerebral blood flow measurements. *Biomed Opt Express*. 2011;2(7):2068-2081. doi:[10.1364/BOE.2.002068](https://doi.org/10.1364/BOE.2.002068)
48. Verdecchia K, Diop M, Lee A, Morrison LB, Lee TY, St Lawrence K. Assessment of a multi-layered diffuse correlation spectroscopy method for monitoring cerebral blood flow in adults. *Biomed Opt Express*. 2016;7(9):3659-3674. doi:[10.1364/BOE.7.003659](https://doi.org/10.1364/BOE.7.003659)
49. Durduran T, Choe R, Baker WB, Yodh AG. Diffuse optics for tissue monitoring and tomography. *Rep Prog Phys*. 2010;73(7):076701. doi:[10.1088/0034-4885/73/7/076701](https://doi.org/10.1088/0034-4885/73/7/076701)
50. Di Giantomasso D, May CN, Bellomo R. Vital organ blood flow during hyperdynamic sepsis. *Chest*. 2003;124(3):1053-1059. doi:[10.1378/chest.124.3.1053](https://doi.org/10.1378/chest.124.3.1053)
51. Bateman RM, Sharpe MD, Ellis CG. Bench-to bedside review: microvascular dysfunction in sepsis—hemodynamics, oxygen transport, and nitric oxide. *Crit Care*. 2003;7(5):359-373. doi:[10.1186/cc2353](https://doi.org/10.1186/cc2353)
52. Intaglietta M. Vasomotion and flowmotion: physiological mechanisms and clinical evidence. *Vasc Med Rev*. 1990;vmr-1(2):101-112. doi:[10.1177/1358836X9000100202](https://doi.org/10.1177/1358836X9000100202)
53. Murphy E, Steenbergen C. Cardioprotection in females: a role for nitric oxide and altered gene expression. *Heart Fail Rev*. 2007;12(3-4):293-300. doi:[10.1007/s10741-007-9035-0](https://doi.org/10.1007/s10741-007-9035-0)
54. Secor D, Li F, Ellis CG, et al. Impaired microvascular perfusion in sepsis requires activated coagulation and P-selectin-mediated platelet adhesion in capillaries. *Intensive Care Med*. 2010;36(11):1928-1934. doi:[10.1007/s00134-010-1969-3](https://doi.org/10.1007/s00134-010-1969-3)
55. Madoiwa S. Recent advances in disseminated intravascular coagulation: endothelial cells and fibrinolysis in sepsis-induced DIC. *J Intensive Care*. 2015;3(1):8. doi:[10.1186/s40560-015-0075-6](https://doi.org/10.1186/s40560-015-0075-6)
56. Piper RD, Pitt-Hyde ML, Anderson LA, Sibbald WJ, Potter RF. Leukocyte activation and flow behavior in rat skeletal muscle in sepsis. *Am J Respir Crit Care Med*. 1998;157(1):129-134. doi:[10.1164/ajrccm.157.1.9609012](https://doi.org/10.1164/ajrccm.157.1.9609012)
57. Lam C, Tynl K, Martin C, Sibbald W. Microvascular perfusion is impaired in a rat model of normotensive sepsis. *J Clin Invest*. 1994;94(5):2077-2083. doi:[10.1172/JCI117562](https://doi.org/10.1172/JCI117562)

58. Tyml K, Yu J, McCormack DG. Capillary and arteriolar responses to local vasodilators are impaired in a rat model of sepsis. *J Appl Physiol*. 1998;84(3):837-844. doi:[10.1152/jappl.1998.84.3.837](https://doi.org/10.1152/jappl.1998.84.3.837)
59. Tyml K. Role of connexins in microvascular dysfunction during inflammation. *Can J Physiol Pharmacol*. 2011;89(1):1-12. doi:[10.1139/Y10-099](https://doi.org/10.1139/Y10-099)
60. Tyml K, Wang X, Lidington D, Ouellette Y. Lipopolysaccharide reduces intercellular coupling in vitro and arteriolar conducted response in vivo. *Am J Physiol-Heart Circulat Physiol*. 2001;281(3):H1397-H1406. doi:[10.1152/ajpheart.2001.281.3.H1397](https://doi.org/10.1152/ajpheart.2001.281.3.H1397)
61. Lidington D, Ouellette Y, Li F, Tyml K. Conducted vasoconstriction is reduced in a mouse model of sepsis. *J Vasc Res*. 2003;40(2):149-158. doi:[10.1159/000070712](https://doi.org/10.1159/000070712)
62. Mckinnon R, Lidington D, Bolon M, Ouellette Y, Kidder G, Tyml K. Reduced arteriolar conducted vasoconstriction in septic mouse cremaster muscle is mediated by nNOS-derived NO. *Cardiovasc Res*. 2006;69(1):236-244. doi:[10.1016/j.cardiores.2005.09.003](https://doi.org/10.1016/j.cardiores.2005.09.003)
63. Meyer C, de Vries G, Davidge ST, Mayes DC. Reassessing the mathematical modeling of the contribution of Vasomotion to vascular resistance. *J Appl Physiol*. 2002;92(2):888-889. doi:[10.1152/jappl.2002.92.2.888](https://doi.org/10.1152/jappl.2002.92.2.888)
64. Dellinger RP, Levy MM, Rhodes A, et al. Surviving sepsis campaign: international guidelines for Management of Severe Sepsis and Septic Shock, 2012. *Intensive Care Med*. 2013;39(2):165-228. doi:[10.1007/s00134-012-2769-8](https://doi.org/10.1007/s00134-012-2769-8)
65. Roger C, Zieleskiewicz L, Demattei C, et al. Time course of fluid responsiveness in sepsis: the fluid challenge revisiting (FCREV) study. *Crit Care*. 2019;23(1):179. doi:[10.1186/s13054-019-2448-z](https://doi.org/10.1186/s13054-019-2448-z)
66. Mohamed AS, Hosney M, Bassiony H, et al. Sodium pentobarbital dosages for exsanguination affect biochemical, molecular and histological measurements in rats. *Sci Rep*. 2020;10(1):378. doi:[10.1038/s41598-019-57252-7](https://doi.org/10.1038/s41598-019-57252-7)
67. Westenberg IS, Bolam JM. Duration of response to pentobarbital of female vs male albino and pigmented rats. *Pharmacol Biochem Behav*. 1982;16(5):815-818. doi:[10.1016/0091-3057\(82\)90241-6](https://doi.org/10.1016/0091-3057(82)90241-6)
68. Wang Z, Schuler B, Vogel O, Arras M, Vogel J. What is the optimal anesthetic protocol for measurements of cerebral autoregulation in spontaneously breathing mice? *Exp Brain Res*. 2010;207:249-258. doi:[10.1007/s00221-010-2447-4](https://doi.org/10.1007/s00221-010-2447-4)
69. Milej D, Abdalmalak A, Desjardins L, et al. Quantification of blood-brain barrier permeability by dynamic contrast-enhanced NIRS. *Sci Rep*. 2017;7:1702. doi:[10.1038/s41598-017-01922-x](https://doi.org/10.1038/s41598-017-01922-x)

SUPPORTING INFORMATION

Additional supporting information can be found online in the Supporting Information section at the end of this article.

How to cite this article: Eskandari R, Milkovich S, Kamar F, et al. Non-invasive point-of-care optical technique for continuous in vivo assessment of microcirculatory function: Application to a preclinical model of early sepsis. *The FASEB Journal*. 2024;38:e70204. doi:[10.1096/fj.202401889R](https://doi.org/10.1096/fj.202401889R)

APPENDIX 1

Table of all the results (mean \pm standard deviations).

Parameter	Control		Septic	
MAP (mmHg)	Male ($n=2$):	Group avg ($n=4$):	Male ($n=5$):	Group avg ($n=10$):
	Hour 0.5:	Hour 0.5:	Hour 0.5:	Hour 0.5:
	96.584 \pm 3.50	98.60 \pm 8.72	113.22 \pm 6.96	116.73 \pm 7.84
	Hour 2:	Hour 2:	Hour 2:	Hour 2:
	88.93 \pm 1.80	88.61 \pm 5.64	102.44 \pm 9.34	102.55 \pm 9.04
	Hour 4:	Hour 4:	Hour 4:	Hour 4:
	98.79 \pm 7.02	91.33 \pm 12.33	90.67 \pm 7.65	83.72 \pm 10.49
	Hour 6:	Hour 6:	Hour 6:	Hour 6:
	93.94 \pm 5.10	90.15 \pm 8.68	67.04 \pm 8.95	67.32 \pm 6.67
	Female ($n=2$):		Female ($n=5$):	
	Hour 0.5:		Hour 0.5:	
	100.61 \pm 14.13		120.23 \pm 7.69	
	Hour 2:		Hour 2:	
	88.28 \pm 9.58		102.66 \pm 9.83	
Hour 4:		Hour 4:		
83.87 \pm 13.58		76.77 \pm 8.28		
Hour 6:		Hour 6:		
86.36 \pm 11.93		67.61 \pm 4.44		

(Continues)

APPENDIX 1 (Continued)

Parameter	Control		Septic	
Lactate (mmol/L)	Male (<i>n</i> = 2):	Group avg (<i>n</i> = 4):	Male (<i>n</i> = 5):	Group avg (<i>n</i> = 10):
	Hour 0.5:	Hour 0.5:	Hour 0.5:	Hour 0.5:
	0.96 ± 0.02	0.86 ± 0.17	1.69 ± 0.30	1.83 ± 0.74
	Hour 2:	Hour 2:	Hour 2:	Hour 2:
	1.13 ± 0.50	0.98 ± 0.35	1.45 ± 0.50	1.80 ± 0.77
	Hour 4:	Hour 4:	Hour 4:	Hour 4:
	0.43 ± 0.10	0.37 ± 0.09	0.99 ± 0.20	0.92 ± 0.26
	Hour 6:	Hour 6:	Hour 6:	Hour 6:
	0.65 ± 0.25	0.49 ± 0.23	1.24 ± 0.19	1.34 ± 0.52
	Female (<i>n</i> = 2):		Female (<i>n</i> = 5):	
	Hour 0.5:		Hour 0.5:	
	0.76 ± 0.23		1.96 ± 1.05	
	Hour 2:		Hour 2:	
	0.84 ± 0.18		2.15 ± 0.90	
	Hour 4:		Hour 4:	
	0.32 ± 0.02		0.86 ± 0.31	
Hour 6:		Hour 6:		
0.33 ± 0.02		1.43 ± 0.74		
Peripheral HbT (μM)	Male (<i>n</i> = 2):	Group avg (<i>n</i> = 4):	Male (<i>n</i> = 5):	Group avg (<i>n</i> = 10):
	Hour 0.5:	Hour 0.5:	Hour 0.5:	Hour 0.5:
	68.77 ± 23.91	65.10 ± 18.25	58.80 ± 19.06	59.03 ± 12.81
	Hour 2:	Hour 2:	Hour 2:	Hour 2:
	70.00 ± 26.45	60.76 ± 26.28	64.88 ± 16.72	66.70 ± 16.38
	Hour 4:	Hour 4:	Hour 4:	Hour 4:
	71.48 ± 23.20	68.70 ± 17.18	56.72 ± 19.64	56.07 ± 13.87
	Hour 6:	Hour 6:	Hour 6:	Hour 6:
	61.24 ± 8.50	60.39 ± 6.04	55.81 ± 22.68	52.33 ± 60.39
	Female (<i>n</i> = 2):		Female (<i>n</i> = 5):	
	Hour 0.5:		Hour 0.5:	
	61.42 ± 19.33		59.27 ± 2.42	
	Hour 2:		Hour 2:	
	51.52 ± 32.12		68.52 ± 17.78	
	Hour 4:		Hour 4:	
	65.93 ± 17.78		55.42 ± 6.76	
Hour 6:		Hour 6:		
59.54 ± 5.86		48.86 ± 14.00		
Peripheral rBF (%)	Male (<i>n</i> = 2):	Group avg (<i>n</i> = 4):	Male (<i>n</i> = 5):	Group avg (<i>n</i> = 10):
	Hour 2:	Hour 2:	Hour 2:	Hour 2:
	105.43 ± 11.82	102.71 ± 9.05	79.06 ± 7.90	72.10 ± 9.54
	Hour 4:	Hour 4:	Hour 4:	Hour 4:
	100.73 ± 0.49	95.67 ± 7.17	63.26 ± 11.34	57.00 ± 10.49
	Hour 6:	Hour 6:	Hour 6:	Hour 6:
	108.72 ± 10.30	99.97 ± 13.32	59.81 ± 13.25	56.29 ± 11.00
	Female (<i>n</i> = 2):		Female (<i>n</i> = 5):	
	Hour 2:		Hour 2:	
	99.98 ± 8.75		65.14 ± 4.64	
	Hour 4:		Hour 4:	
	90.61 ± 7.20		50.74 ± 4.59	
	Hour 6:		Hour 6:	
	91.23 ± 10.97		52.77 ± 8.09	

APPENDIX 1 (Continued)

Parameter	Control	Septic		
Peripheral StO ₂ (%)	Male (n=2):	Group avg (n=4):	Male (n=5):	Group avg (n=10):
	Hour 0.5:	Hour 0.5:	Hour 0.5:	Hour 0.5:
	76.70 ± 4.09	78.73 ± 8.24	74.61 ± 7.96	78.68 ± 7.10
	Hour 2:	Hour 2:	Hour 2:	Hour 2:
	74.00 ± 3.65	73.61 ± 13.24	72.66 ± 8.28	74.67 ± 7.99
	Hour 4:	Hour 4:	Hour 4:	Hour 4:
	74.46 ± 0.11	73.63 ± 13.22	71.85 ± 8.29	72.97 ± 7.44
	Hour 6:	Hour 6:	Hour 6:	Hour 6:
	75.23 ± 3.49	74.04 ± 13.44	72.22 ± 7.80	73.54 ± 6.89
	Female (n=2):		Female (n=5):	
	Hour 0.5:		Hour 0.5:	
	80.77 ± 13.05		82.75 ± 2.94	
	Hour 2:		Hour 2:	
	73.22 ± 22.62		76.67 ± 8.07	
Hour 4:		Hour 4:		
72.80 ± 22.83		74.09 ± 7.26		
Hour 6:		Hour 6:		
72.86 ± 22.90		74.87 ± 6.45		
Cerebral HbT (μM)	Male (n=2):	Group avg (n=4):	Male (n=5):	Group avg (n=10):
	Hour 0.5:	Hour 0.5:	Hour 0.5:	Hour 0.5:
	76.39 ± 16.62	62.87 ± 20.16	73.40 ± 21.37	85.99 ± 26.12
	Hour 2:	Hour 2:	Hour 2:	Hour 2:
	70.38 ± 17.80	52.86 ± 30.33	61.76 ± 23.69	72.59 ± 34.45
	Hour 4:	Hour 4:	Hour 4:	Hour 4:
	71.50 ± 20.80	57.39 ± 25.61	65.30 ± 8.26	74.62 ± 30.65
	Hour 6:	Hour 6:	Hour 6:	Hour 6:
	72.42 ± 23.12	56.49 ± 24.77	67.86 ± 24.67	75.82 ± 30.59
	Female (n=2):		Female (n=5):	
	Hour 0.5:		Hour 0.5:	
	49.35 ± 14.57		98.62 ± 26.07	
	Hour 2:		Hour 2:	
	35.34 ± 34.87		83.43 ± 42.61	
Hour 4:		Hour 4:		
43.28 ± 27.18		83.95 ± 42.76		
Hour 6:		Hour 6:		
40.56 ± 17.05		83.78 ± 36.58		
Cerebral rBF (%)	Male (n=2):	Group avg (n=4):	Male (n=5):	Group avg (n=10):
	Hour 2:	Hour 2:	Hour 2:	Hour 2:
	107.794 ± 11.340	106.95 ± 28.42	89.72 ± 16.97	87.40 ± 23.29
	Hour 4:	Hour 4:	Hour 4:	Hour 4:
	96.97 ± 8.08	101.00 ± 23.64	71.27 ± 18.91	68.41 ± 18.29
	Hour 6:	Hour 6:	Hour 6:	Hour 6:
	91.25 ± 17.33	101.40 ± 31.52	55.70 ± 12.94	59.92 ± 20.13
	Female (n=2):		Female (n=5):	
	Hour 2:		Hour 2:	
	106.10 ± 47.87		85.08 ± 30.32	
	Hour 4:		Hour 4:	
	105.03 ± 39.33		65.54 ± 19.36	
	Hour 6:		Hour 6:	
	111.55 ± 47.63		64.15 ± 26.46	

(Continues)

APPENDIX 1 (Continued)

Parameter	Control		Septic	
Peripheral StO ₂ (%)	Male (n=2):	Group avg (n=4):	Male (n=5):	Group avg (n=10):
	Hour 0.5:	Hour 0.5:	Hour 0.5:	Hour 0.5:
	71.65 ± 0.33	69.16 ± 10.70	70.22 ± 17.93	72.13 ± 13.82
	Hour 2:	Hour 2:	Hour 2:	Hour 2:
	70.24 ± 1.09	62.98 ± 21.63	62.33 ± 21.49	64.79 ± 18.39
	Hour 4:	Hour 4:	Hour 4:	Hour 4:
	71.73 ± 1.89	62.51 ± 23.92	60.78 ± 20.39	62.99 ± 17.52
	Hour 6:	Hour 6:	Hour 6:	Hour 6:
	71.34 ± 5.44	64.85 ± 19.02	54.75 ± 25.59	59.54 ± 20.90
	Female (n=2):		Female (n=5):	
	Hour 0.5:		Hour 0.5:	
	66.68 ± 17.86		74.03 ± 9.96	
	Hour 2:		Hour 2:	
	55.71 ± 34.51		67.25 ± 16.85	
Hour 4:		Hour 4:		
53.29 ± 37.06		65.20 ± 16.22		
Hour 6:		Hour 6:		
58.36 ± 29.78		64.33 ± 16.45		
Power of peripheral HbT (μM) oscillation	Male (n=2):	Group avg (n=4):	Male (n=5):	Group avg (n=10):
	Period 1:	Period 1:	Period 1:	Period 1:
	0.09 ± 0.02	0.11 ± 0.03	0.21 ± 0.07	0.16 ± 0.09
	Period 2:	Period 2:	Period 2:	Period 2:
	0.10 ± 0.02	0.13 ± 0.05	0.48 ± 0.13	0.41 ± 0.21
	Period 3:	Period 3:	Period 3:	Period 3:
	0.12 ± 0.004	0.17 ± 0.08	0.71 ± 0.12	0.64 ± 0.27
	Female (n=2):		Female (n=5):	
	Period 1:		Period 1:	
	0.13 ± 0.02		0.10 ± 0.09	
Period 2:		Period 2:		
0.15 ± 0.07		0.33 ± 0.25		
Period 3:		Period 3:		
0.22 ± 0.09		0.58 ± 0.37		
Power of Peripheral StO ₂ (%) Oscillation	Male (n=2):	Group avg (n=4):	Male (n=5):	Group avg (n=10):
	Period 1:	Period 1:	Period 1:	Period 1:
	0.07 ± 0.04	0.09 ± 0.07	0.19 ± 0.07	0.13 ± 0.08
	Period 2:	Period 2:	Period 2:	Period 2:
	0.07 ± 0.03	0.08 ± 0.03	0.44 ± 0.24	0.39 ± 0.23
	Period 3:	Period 3:	Period 3:	Period 3:
	0.09 ± 0.02	0.10 ± 0.04	0.64 ± 0.40	0.64 ± 0.41
	Female (n=2):		Female (n=5):	
	Period 1:		Period 1:	
	0.12 ± 0.10		0.07 ± 0.04	
Period 2:		Period 2:		
0.08 ± 0.03		0.33 ± 0.23		
Period 3:		Period 3:		
0.12 ± 0.05		0.65 ± 0.46		

APPENDIX 1 (Continued)

Parameter	Control		Septic	
Power of peripheral rBF (%) oscillation	Male (n = 2):	Group avg (n = 4):	Male (n = 5):	Group avg (n = 10):
	Period 1:	Period 1:	Period 1:	Period 1:
	1.43 ± 0.19	1.21 ± 0.29	1.37 ± 0.09	1.31 ± 0.27
	Period 2:	Period 2:	Period 2:	Period 2:
	1.46 ± 0.27	1.31 ± 0.24	2.51 ± 0.49	2.06 ± 0.58
	Period 3:	Period 3:	Period 3:	Period 3:
	1.89 ± 0.81	1.62 ± 0.57	3.29 ± 0.76	2.68 ± 0.92
	Female (n = 2):		Female (n = 5):	
	Period 1:		Period 1:	
	0.99 ± 0.16		1.25 ± 0.39	
	Period 2:		Period 2:	
	1.16 ± 0.12		1.62 ± 0.19	
	Period 3:		Period 3:	
	1.34 ± 0.10		2.07 ± 0.63	
Power of cerebral HbT (µM) Oscillation	Male (n = 2):	Group avg (n = 4):	Male (n = 5):	Group avg (n = 10):
	Period 1:	Period 1:	Period 1:	Period 1:
	0.08 ± 0.01	0.06 ± 0.03	0.10 ± 0.03	0.07 ± 0.03
	Period 2:	Period 2:	Period 2:	Period 2:
	0.09 ± 0.003	0.06 ± 0.03	0.20 ± 0.09	0.15 ± 0.08
	Period 3:	Period 3:	Period 3:	Period 3:
	0.11 ± 0.04	0.08 ± 0.04	0.36 ± 0.11	0.26 ± 0.13
	Female (n = 2):		Female (n = 5):	
	Period 1:		Period 1:	
	0.04 ± 0.03		0.05 ± 0.01	
	Period 2:		Period 2:	
	0.04 ± 0.03		0.10 ± 0.04	
	Period 3:		Period 3:	
	0.05 ± 0.02		0.15 ± 0.03	
Power of cerebral StO ₂ (%) oscillation	Male (n = 2):	Group avg (n = 4):	Male (n = 5):	Group avg (n = 10):
	Period 1:	Period 1:	Period 1:	Period 1:
	0.07 ± 0.04	0.09 ± 0.09	0.15 ± 0.15	0.10 ± 0.11
	Period 2:	Period 2:	Period 2:	Period 2:
	0.11 ± 0.03	0.13 ± 0.09	0.24 ± 0.23	0.17 ± 0.18
	Period 3:	Period 3:	Period 3:	Period 3:
	0.13 ± 0.02	0.14 ± 0.07	0.31 ± 0.21	0.21 ± 0.18
	Female (n = 2):		Female (n = 5):	
	Period 1:		Period 1:	
	0.12 ± 0.14		0.05 ± 0.04	
	Period 2:		Period 2:	
	0.15 ± 0.15		0.11 ± 0.08	
	Period 3:		Period 3:	
	0.15 ± 0.12		0.11 ± 0.06	
Power of cerebral rBF (%) oscillation	Male (n = 2):	Group avg (n = 4):	Male (n = 5):	Group avg (n = 10):
	Period 1:	Period 1:	Period 1:	Period 1:
	1.29 ± 0.11	1.21 ± 0.13	1.06 ± 0.13	1.06 ± 0.21
	Period 2:	Period 2:	Period 2:	Period 2:
	1.20 ± 0.12	1.31 ± 0.21	1.17 ± 0.12	1.18 ± 0.18
	Period 3:	Period 3:	Period 3:	Period 3:
	1.23 ± 0.04	1.31 ± 0.17	1.33 ± 0.30	1.37 ± 0.27
	Female (n = 2):		Female (n = 5):	
	Period 1:		Period 1:	
	1.12 ± 0.10		1.05 ± 0.29	
	Period 2:		Period 2:	
	1.42 ± 0.28		1.19 ± 0.24	
	Period 3:		Period 3:	
	1.40 ± 0.24		1.42 ± 0.26	